2007

Blind colour isolation for colour-channel-based fringe pattern profilometry using digital projection

Y. Hu
University of Wollongong, yingsong@uow.edu.au

Jiangtao Xi
University of Wollongong, jiangtao@uow.edu.au

Joe F. Chicharo
University of Wollongong, chicharo@uow.edu.au

Zongkai Yang
Huazhong University of Science and Technology

Blind colour isolation for colour-channel-based fringe pattern profilometry using digital projection

Abstract

We present an algorithm for estimating the color demixing matrix based on the color fringe patterns captured from the reference plane or the surface of the object. The advantage of this algorithm is that it is a blind approach to calculating the demixing matrix in the sense that no extra images are required for color calibration before performing profile measurement. Simulation and experimental results convince us that the proposed algorithm can significantly reduce the influence of the color cross talk and at the same time improve the measurement accuracy of the color-channel-based phase-shifting profilometry.

Disciplines

Physical Sciences and Mathematics

Publication Details

Hu, Y., Xi, J., Chicharo, J. F. & Yang, Z. (2007). Blind colour isolation for colour-channel-based fringe pattern profilometry using digital projection. Journal A of the Optical Society of America: Optics, Image Science, and Vision, 24 (8), 2372-2382.

Blind color isolation for color-channel-based fringe pattern profilometry using digital projection

Yingsong Hu,[1,2,*] Jiangtao Xi,[1,2] Joe Chicharo,[1] and Zongkai Yang[2]

[1]*School of Electrical Computer and Telecommunications Engineering, University of Wollongong, NSW 2522, Australia*

[2]*Department of Electronics and Information Engineering, Huazhong University of Science and Technology, Wuhan City, 430074, China*

[*]*Corresponding author: yingsong@uow.edu.au*

Received June 1, 2006; revised February 2, 2007; accepted March 13, 2007; posted March 26, 2007 (Doc. ID 71611); published July 11, 2007

We present an algorithm for estimating the color demixing matrix based on the color fringe patterns captured from the reference plane or the surface of the object. The advantage of this algorithm is that it is a blind approach to calculating the demixing matrix in the sense that no extra images are required for color calibration before performing profile measurement. Simulation and experimental results convince us that the proposed algorithm can significantly reduce the influence of the color cross talk and at the same time improve the measurement accuracy of the color-channel-based phase-shifting profilometry. © 2007 Optical Society of America

OCIS codes: 120.6650, 120.2650, 150.6910.

1. INTRODUCTION

Fringe pattern profilometry (FPP) is one of the most popular noncontact approaches to measuring three-dimensional object surfaces. With FPP, a Ronchi grating or sinusoidal grating is projected onto a three-dimensional diffuse surface, the height distribution of which deforms the projected fringe patterns and modulates them in the phase domain. Hence by retrieving the phase difference between the original and the deformed fringe patterns, three-dimensional profilometry can be achieved. To obtain phase maps from original and deformed fringes patterns, researchers have contributed various analysis methods, including Fourier transform profilometry (FTP) [1–6], phase-shifting profilometry (PSP) [7–9], spatial phase detection (SPD) [10], phase-locked loop (PLL) [11] and other analysis methods [12,13].

Among these methods, FTP and PSP are two of the most popular and typical algorithms to implement profilometry. The most important advantage of FTP is that it requires only one image frame for each measured object, which is very suitable for real-time applications. However, the disadvantage of FTP is its sensitivity to the background and the reflection property of the object surface. In contrast to FTP, PSP is more precise and less sensitive to the background and the reflection factor of object surfaces. However, it is not suitable for dynamic measurement, because with PSP, phase-stepped fringe patterns are sequentially projected onto objects and acquired by a CCD camera. Obviously, the sequential projection of the phase-stepped fringe patterns requires time. To overcome the shortcomings of the PSP method, the color-channel-based PSP approach [14] has been presented, in which the phase-stepped fringes are simultaneously projected through different color channels (Red, Green, and Blue), respectively, so that three phase-stepped fringe patterns can be projected and recorded within a colored fringe pattern image synchronously. Thus, theoretically, it becomes possible to develop real-time applications using the PSP algorithm. However, color cross talk among the channels will introduce measurement errors when using the color-channel-based PSP method. Therefore, the color isolation process is considered essential before using the PSP algorithm to effectively reconstruct the surface.

To eliminate the color cross talk, a linear mixing model and relevant calibration method has been utilized in [15], in which the color mixing process is modeled by a mixing matrix and at least nine extra images are introduced to determine the elements of the mixing matrix in the whole calibration process. Further, in order to reduce the number of the images required for the calibration procedure, Hu *et al.* [16] proposed a calibration method based on a blind signal separation algorithm to calculate the color demixing matrix, by which only one colored image with independent signals in each channel is projected and recorded for the color demixing calibration. However, an extra image is still required to determine the mixing matrix or the demixing matrix. Moreover, any calibration method has the drawback that if the condition of the system changes, the calibration process has to be performed again.

Motivated by the problem of calibration-based methods, in this paper we propose an algorithm, called blind color isolation (BCI) method, to adaptively determine the demixing matrix without any prior knowledge of the system or using any probing signals. The BCI algorithm determines the demixing matrix by using the projected colored fringe patterns only on the reference plane, and no extra images are introduced for color calibration. Our simulation and experimental results show that the color leakage can be adaptively reduced and accordingly the measurement accuracy using the color-channel-based PSP method can be significantly improved.

1084-7529/07/082372-11/$15.00

This paper is organized as follows. In Section 2, we review the principles of the PSP technique and the color-channel-based PSP method. In Section 3, the influence of color cross talk is mathematically modeled and analyzed. Based on the analysis, the color demixing scheme is proposed. In Section 4, the BCI algorithm is derived to adaptively determine the demixing matrix. Simulation and experimental results are demonstrated in Section 5. Section 6 concludes this paper.

2. PRINCIPLES ASSOCIATED WITH COLOR-CHANNEL-BASED PSP

A schematic diagram of a typical FPP system is shown in Fig. 1. For simplicity, we consider a cross section of the object surface for a given y coordinate. Hence, the intensity of fringe patterns captured by the CCD camera and the height distribution function can be expressed as a function with a single variable x. Thus we use $s(x)$ and $d(x)$ to denote the intensity of the projected and the deformed fringe pattern, respectively, and use $h(x)$ to represent the height distribution of the object surface.

In the PSP approach, M ($M \geq 3$) fringe patterns are sequentially projected onto the reference plane and the surface of the object and then captured by a CCD camera. Each one of the M fringe patterns has phase difference of $2\pi/M$ from its adjacent patterns. Thus, the projected fringe patterns $s_m(x)$ and $d_m(x)$ can be expressed as [17]

$$s_m(x) = b_0 + b_1 \cos\left(2\pi f_0 x + \frac{2\pi(m-1)}{M}\right) \quad \text{for } m = 1,2,\ldots,M, \tag{1}$$

$$d_m(x) = b_0 + b_1 \cos\left(2\pi f_0 x + \frac{2\pi(m-1)}{M} + \phi(x)\right) \quad \text{for } m = 1,2,\ldots,M, \tag{2}$$

where b_0 is the background illumination and b_1 represents the contrast between bright and dark fringes. $\phi(x)$ is the phase shift caused by the height distribution of the object surface. The phase map $\phi(x)$ and the height distribution of the object $h(x)$ can be calculated by following equations:

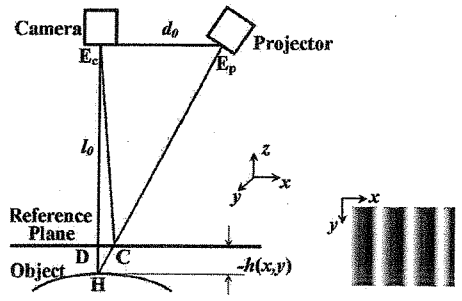

Fig. 1. Schematic diagram of the FPP system.

$$S = \tan(2\pi f_0 x) = -\frac{\sum_{m=1}^{M} s_m(x)\sin(2\pi(m-1)/M)}{\sum_{m=1}^{M} s_m(x)\cos(2\pi(m-1)/M)}, \tag{3}$$

$$D = \tan(2\pi f_0 x + \phi(x)) = -\frac{\sum_{m=1}^{M} d_m(x)\sin(2\pi(m-1)/M)}{\sum_{m=1}^{M} d_m(x)\cos(2\pi(m-1)/M)}, \tag{4}$$

$$\phi(x) = unwrap(\arctan(D)) - unwrap(\arctan(S)), \tag{5}$$

$$h(x) = \frac{l_0\phi(x)}{\phi(x) - 2\pi f_0 d_0}, \tag{6}$$

where S and D are intermediate variables; d_0 and l_0 are the distances from the camera to the projector and the reference plane, respectively; f_0 is the spatial frequency of the fringe patterns and *unwrap* denotes the operation of phase unwrapping.

As mentioned in Section 1, the disadvantage of traditional PSP is that at least three frames of images are required to implement profilometry, while sequential projection of fringe patterns takes a relatively long time, which makes the PSP unsuitable for real-time applications. To solve this problem, the color-channel-based approach has been presented [14]. In color-channel-based PSP, three phase-shifted fringe patterns with $2\pi/3$ difference from one another are projected through the three fundamental color channels (Red, Green, and Blue) and captured by a color CCD, so that three phase shifted fringe patterns can be simultaneously projected and recorded in a color fringe image. Hence, a real-time PSP measurement technique can be implemented. However, because the isolation of the color channels cannot be perfect, color cross talk always exists, which will certainly result in measurement errors. In the next section, the color cross-talk phenomenon will be mathematically modeled and theoretically analyzed. Based on the analysis, a blind color-isolation algorithm is proposed.

3. ANALYSIS OF THE COLOR CROSS-TALK PHENOMENON

A. Notation and Definitions

For simplicity, assuming the length of signal $s_m(x)$ is N, we can use an $M \times N$ matrix to represent a set of signals $\mathbf{s}_m$ for $m = 1,2,\ldots,M$, i.e.,

$$\mathbf{s} = (s_{m,n})_{M\times N}, \tag{7}$$

where $s_{m,n} = s_m(n)$, $m = 1,2\ldots,M$ and $n = 1,2,\ldots,N$. Further, $\mathbf{s}_m$ denotes the mth row vector of the matrix $\mathbf{s}$, and $\mathbf{s}(n)$ represents the nth column vector of $\mathbf{s}$.

In addition, let us recall the projected signals expressed by Eq. (1): $\mathbf{s}$ is actually a set of very particular signals. In order to describe and name this kind of signal sets, a definition is given:

Definition 1. For a set of signals $v_m(x) = b_{m,0} + b_{m,1}\cos[\theta(x) + \alpha_m]$ $(m = 1,2,\ldots,M, 0 \leq \alpha_1 < \alpha_2 \ldots < \alpha_m < \ldots < \alpha_M < 2\pi, \theta(x) = 2\pi f_0 x)$, if at any point x we have

$$b_{m,0} = b_0 \text{ (where } m = 1,2,\ldots,M \text{ and } b_0 \text{ is a constant)}, \quad (8)$$

$$b_{m,1} = b_1 \text{ (where } m = 1,2,\ldots,M \text{ and } b_1 \text{ is a constant)}, \quad (9)$$

$$\alpha_{m+1} - \alpha_m = 2\pi/M \text{ (where } m = 1,2,\ldots,M-1), \quad (10)$$

we call these M signals a set of "balanced" signals or M "balanced" signals; otherwise, they are called "unbalanced."

Obviously, according to this definition, $\mathbf{s}$ is a set of balanced signals.

In addition, although greater phase-shift steps will provide better reconstruction accuracy for normal PSP [18], the only choice for color-channel-based PSP is to use three steps, because as introduced in Section 2 only three fundamental colors are available to independently carry phase shifted fringe patterns. Therefore, in this paper we consider only the case where $M=3$.

B. Linear Mixing Model

In this subsection, first, to analyze the color cross talk, we assume that there is no nonlinear distortion in the system. Furthermore, in Subsection 3.C we discuss a more general model where nonlinear distortions are taken into consideration.

Without nonlinear distortion, a color mixing process can be modeled by a mixing matrix [15,16]; i.e., the captured fringe patterns can be expressed as

$$\hat{\mathbf{s}} = \mathbf{A}\mathbf{s}, \quad (11)$$

where $\mathbf{A}$ is a 3×3 matrix, which we call a mixing matrix, and $\hat{\mathbf{s}}$ denotes the mixed fringe patterns captured on the reference plane. For simplicity, let $\theta(x)$ represent $2\pi f_0 x$; with this notation, the mth row of $\hat{\mathbf{s}}$ may be rewritten as

$$\begin{aligned}
\hat{\mathbf{s}}_m &= \mathbf{A}_m\mathbf{s} \\
&= a_{m,1}(b_0 + b_1\cos\theta(x)) + a_{m,2}\left(b_0 + b_1\cos\left(\theta(x) + \frac{2\pi}{3}\right)\right) \\
&\quad + a_{m,3}\left(b_0 + b_1\cos\left(\theta(x) + \frac{4\pi}{3}\right)\right) \\
&= b_0(a_{m,1} + a_{m,2} + a_{m,3}) + b_1\left[a_{m,1}\cos\theta(x)\right. \\
&\quad + a_{m,2}\left(\cos\theta(x)\cos\frac{2\pi}{3} - \sin\theta(x)\sin\frac{2\pi}{3}\right) \\
&\quad \left. + a_{m,3}\left(\cos\theta(x)\cos\frac{4\pi}{3} - \sin\theta(x)\sin\frac{4\pi}{3}\right)\right] \\
&= b_0(a_{m,1} + a_{m,2} + a_{m,3}) + b_1\left[\left(a_{m,1} - \frac{1}{2}a_{m,2}\right.\right. \\
&\quad \left.\left. - \frac{1}{2}a_{m,3}\right)\cos\theta(x) - \frac{\sqrt{3}}{2}(a_{m,2} - a_{m,3})\sin\theta(x)\right] \\
&= \hat{b}_{m,0} + \hat{b}_{m,1}\cos(\theta(x) + \hat{\alpha}_m), \quad (12)
\end{aligned}$$

where

$$\hat{b}_{m,0} = b_0(a_{m,1} + a_{m,2} + a_{m,3}),$$

$$\begin{aligned}
\hat{b}_{m,1} &= b_1\sqrt{\left(a_{m,1} - \frac{1}{2}a_{m,2} - \frac{1}{2}a_{m,3}\right)^2 + \frac{3}{4}(a_{m,2} - a_{m,3})^2} \\
&= b_1\sqrt{\frac{1}{2}[(a_{m,1} - a_{m,2})^2 + (a_{m,2} - a_{m,3})^2 + (a_{m,1} - a_{m,3})^2]},
\end{aligned}$$

$$\tan(\hat{\alpha}_m) = \frac{\sqrt{3}(a_{m,2} - a_{m,3})}{2a_{m,1} - a_{m,2} - a_{m,3}}. \quad (13)$$

It can be seen that after the color cross talk, the frequency of the fringe pattern remains unchanged, but usually the contrast, the phase, and the dc components of the fringe patterns in each channel are changed. Additionally, as component $\hat{b}_{m,0}$ does not contain any phase information and can be easily removed by subtracting the mean value of $\hat{\mathbf{s}}_m$, for simplicity we assume that the captured fringe patterns are preprocessed such that they all have zero means before other signal processing operations are applied. Thus, after removing the dc components, the "zero-mean" $\hat{\mathbf{s}}$ can be expressed as

$$\hat{\mathbf{s}}_m = \hat{b}_{m,1}\cos(\theta(x) + \hat{\alpha}_m) \quad \text{for } m = 1,2,3. \quad (14)$$

Note that although the dc components have been removed, signal set $\hat{\mathbf{s}}$ generally remains unbalanced still, because $\hat{b}_m$ and $\hat{\alpha}_m$ usually do not satisfy the conditions in Definition 1. In general, $\hat{s}$ is unbalanced, since the mixing matrices would be different from system to system. That is, the color cross talk will unbalance the original balanced signal set. Therefore, simply treating $\hat{\mathbf{s}}$ as balanced signals and using Eqs. (3)–(5) to calculate phase shift $\phi(x)$ will result in errors.

As the color cross-talk matrix $\mathbf{A}$ is unknown, $\hat{\alpha}_m$ and $\hat{b}_m$ are also unknown. Therefore, retrieving $\phi(x)$ from $\hat{\mathbf{s}}$ is equivalent to reconstructing the phase map from the fringe patterns with unknown phase shifts. To solve this problem, various approaches have been proposed [19–27]. However, as discussed in [26,27], some of these methods [19,20] assume that phase shifts are arbitrary but known or the same, and for the other algorithms retrieving phase with unknown phase shifts [21–24], substantial computation loads are usually required, and some methods need as many as 15 interferograms [23] or an additional optical device [22,24]. Recently, an approach to calculating the unknown phase shifts by use of measured object and reference wave intensities has been suggested [25], but it can be used only for pure phase objects, and the approximate values of the phase steps are still required [26]. In addition, in [27] it is pointed out that approaches proposed in [25,26] require measurements of the object and the reference wave intensities; i.e., $\hat{b}_{m,1}$ in Eq. (14) need to be known. Meanwhile, the method proposed in [27] works only for the case where the contrasts of the fringe patterns $b_{m,1}$ have the same values for $m=1,2,3$, which would be a reasonable assumption for normal PSP applications because for normal PSP, the fringe patterns are generated by the same equipment. However, for color-channel-based PSP, every channel has different gain fac-

tors, and, as analyzed above, color cross talk will change all the parameters of the signals except for the fundamental frequency. Therefore, in order to eliminate the errors introduced by the color leakage, we need a new method to demix the cross-talked fringe patterns with arbitrary, unknown amplitudes and phase shifts.

It is not difficult to see that as long as balanced signals are utilized, no errors will be introduced for the retrieval of the phase map. Since the mixing matrix **A** results in the output signal $\hat{\mathbf{s}}$ being unbalanced, a straightforward way is to find a demixing matrix **W** to make the output signal set $\tilde{\mathbf{s}}$ rebalanced:

$$\tilde{\mathbf{s}} = \mathbf{W}\hat{\mathbf{s}} = \mathbf{W}(\mathbf{A}\mathbf{s}) = \mathbf{W}\mathbf{A}\mathbf{s} = \mathbf{L}\mathbf{s}, \tag{15}$$

where $\mathbf{L}=\mathbf{W}\mathbf{A}$ and $\tilde{\mathbf{s}}$ is a set of balanced signals. As **L** is also a 3×3 matrix, similarly to Eq. (14), $\tilde{\mathbf{s}}$ can be expressed as

$$\tilde{\mathbf{s}}_m = \tilde{b}_{m,1}\cos(\theta(x) + \tilde{\alpha}_m), \quad \text{for } m = 1,2,3. \tag{16}$$

Obviously, if the mixing matrix **A** is not ill-conditioned, this problem is always solvable, for example, $\mathbf{W}=\mathbf{A}^{-1}$, where $\mathbf{A}^{-1}$ denotes the inverse matrix of **A**. Meanwhile, $\mathbf{W}=\mathbf{A}^{-1}$ is not the unique solution of this problem, because the only requirement is that $\tilde{\mathbf{s}}$ be balanced. Therefore, we need to find only one of the solutions **W** that can make the output signals $\tilde{\mathbf{s}}$ satisfy the balance conditions:

$$\tilde{b}_{1,1} = \tilde{b}_{2,1} = \tilde{b}_{3,1} = \tilde{b}_1, \tag{17}$$

$$\tilde{\alpha}_3 - \tilde{\alpha}_2 = \tilde{\alpha}_2 - \tilde{\alpha}_1 = 2\pi/3. \tag{18}$$

C. Nonlinear Mixing Model

In the previous subsection, we discovered that the linear mixing of original signals will cause the captured signals to be unbalanced. In this subsection, we will consider a more practical and realistic case where nonlinear distortions exist in both the projection and the CCD system.

A general model describing the whole image projection and acquisition process for fringe pattern profilometry is shown in Fig. 2. The original signal set **s** is first distorted by a nonlinear function f, then mixed by an unknown matrix **A**, and finally nonlinearly distorted again by function g. The nonlinear functions f and g correspond to the nonlinear distortions introduced by the projector and the CCD, respectively, and the matrix **A** represents the color cross-talk process. Based on the new model, a demixing scheme is also proposed in Fig. 2. As color-channel-based PSP is actually a three-step PSP method, which is very sensitive to the second-order harmonic [28], low-pass filters will usually be utilized to extract dc and fundamental components and eliminate higher-order harmonics [17], which are indicated by **LP**s in Fig. 2.

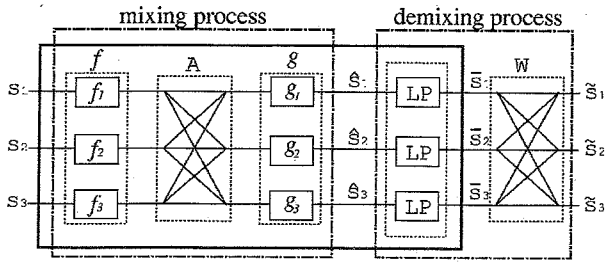

Fig. 2. Nonlinear mixing and demixing.

It can be proved that the nonlinear functions and the color mixing process introduce harmonic components only into the output signal $\hat{\mathbf{s}}$ (see Appendix A for proof). Consequently, $\hat{\mathbf{s}}$ can be expressed as

$$\hat{s}_m(x) = \sum_{k=0}^{K} \hat{b}_{m,k}\cos[k\cdot(\theta(x) + \hat{\alpha}_m)], \quad \text{for } m = 1,2,3, \tag{19}$$

where $\hat{b}_{m,k}$ is the amplitude of the kth harmonic in the mth channel and K is a sufficiently large positive integer. Therefore, after $\hat{\mathbf{s}}$ has been zero-meaned and passed through the low-pass filters, $\bar{\mathbf{s}}$, the fundamental component of $\hat{\mathbf{s}}$ can be obtained and expressed as

$$\bar{s}_m(x) = \hat{b}_{m,1}\cos(\theta(x) + \hat{\alpha}_m), \quad \text{for } m = 1,2,3, \tag{20}$$

where $\hat{b}_{m,1}$ and $\hat{\alpha}_m$ are unknown. Comparing Eq. (20) with Eq. (14) and recalling the problem discussed in Subsection 3.B, it can be noticed that after the fundamental components have been picked up by the low-pass filters, the problem of nonlinear color mixing becomes identical to the problem of the linear mixing case, i.e., the problem of estimating a demixing matrix **W** that balances a set of unbalanced signals. In the next section, we will derive an algorithm for estimating **W**.

4. DERIVATION OF THE BCI ALGORITHM

As analyzed above, the color demixing problem can be converted to an estimation problem where given a set of unbalanced zero-mean signals $\bar{\mathbf{s}}$, we need to estimate a matrix **W** such that $\tilde{\mathbf{s}}=\mathbf{W}\bar{\mathbf{s}}$ is balanced, where $\bar{\mathbf{s}}$ is in the form of Eq. (20).

In order to obtain a set of balanced signals, we have to mathematically describe the characteristics of balanced signals as an objective function, and by minimizing the objective function, **W** can be calculated. Equations (17) and (18) can be a good criterion of a set of three balanced signals, but they are not suitable for estimating **W** because $\hat{b}_{m,1}$ and $\hat{\alpha}_m$ are unknown during the estimation process. Therefore, we have to find an equivalent expression to describe the properties of balanced signals.

It can be proved that a necessary and sufficient condition for the output signals $\tilde{\mathbf{s}}=\mathbf{W}\bar{\mathbf{s}}$ to represent a set of three balanced signals is to ensure that $\tilde{\mathbf{s}}$ satisfies the following two equations (see Appendix B for proof):

$$\mathbf{q}\cdot\tilde{\mathbf{s}}(x) = 0 \text{ for any given } x, \tag{21}$$

$$\tilde{\mathbf{s}}(x)\cdot\tilde{\mathbf{s}}(x) = c \text{ for any given } x, \tag{22}$$

where $\mathbf{q}$ is a column vector $(1,1,1)^{\mathrm{T}}$ and c is a positive constant. The operator $\cdot$ represents an inner product of two vectors.

Based on the equivalent description expressed by Eqs. (21) and (22), an objective function J can be designed as follows:

$$J = J_1 + J_2, \tag{23}$$

where

$$J_1 = [\mathbf{q} \cdot \tilde{\mathbf{s}}(x)]^2, \tag{24}$$

$$J_2 = [\tilde{\mathbf{s}}(x) \cdot \tilde{\mathbf{s}}(x) - c]^2. \tag{25}$$

Note that c is an arbitrarily selected positive constant. In fact, the choice of c affects only the expected amplitude of the demixed signal set but does not influence the balance of the phase. For example, if we expect the amplitude of the rebalanced signal to be 10, according to Eq. (B6) in Appendix B we will have $c=150$.

Therefore, a general algorithm for estimating $\mathbf{W}$ can be derived by a gradient-based method as

$$\hat{\mathbf{W}}_{\mathbf{p}+1} = \hat{\mathbf{W}}_{\mathbf{p}} - \eta \cdot \nabla_{\mathbf{W}} J(\hat{\mathbf{W}}_{\mathbf{p}}), \tag{26}$$

where $\nabla_{\mathbf{W}} J(\cdot)$ denotes the gradient of function $J(\cdot)$ with respect to the demixng matrix $\mathbf{W}$, η is the learning rate, and the subscript $\mathbf{p}$ represents the $\mathbf{p}$th iteration; i.e., $\hat{\mathbf{W}}_p$ is the $\mathbf{p}$th estimate of $\mathbf{W}$. The gradient $\nabla_{\mathbf{W}} J$ can be derived as follows:

$$\nabla_{\mathbf{W}} J = \nabla_{\mathbf{W}} J_1 + \nabla_{\mathbf{W}} J_2. \tag{27}$$

As $\tilde{\mathbf{s}} = \mathbf{W}\bar{\mathbf{s}}$, we have

$$\begin{aligned}\nabla_{\mathbf{W}} J_1 &= \nabla_{\mathbf{W}}[\mathbf{q} \cdot \tilde{\mathbf{s}}(x)]^2 = \nabla_{\mathbf{W}}[\mathbf{q}^{\mathbf{T}}\tilde{\mathbf{s}}(x)]^2 = 2[\mathbf{q}^{\mathbf{T}}\tilde{\mathbf{s}}(x)]\nabla_{\mathbf{W}}[\mathbf{q}^{\mathbf{T}}\tilde{\mathbf{s}}(x)] \\ &= 2[\mathbf{q}^{\mathbf{T}}\mathbf{W}\bar{\mathbf{s}}(x)]\nabla_{\mathbf{W}}[\mathbf{q}^{\mathbf{T}}\mathbf{W}\bar{\mathbf{s}}(x)] = 2[\mathbf{q}^{\mathbf{T}}\mathbf{W}\bar{\mathbf{s}}(x)][\mathbf{q}\bar{\mathbf{s}}^{\mathbf{T}}(x)],\end{aligned} \tag{28}$$

where $(\cdot)^{\mathbf{T}}$ represents transpose. For function J_2, we have

$$\begin{aligned}\nabla_{\mathbf{W}} J_2 &= \nabla_{\mathbf{W}}[\tilde{\mathbf{s}}(x) \cdot \tilde{\mathbf{s}}(x) - c]^2 \\ &= 2[\tilde{\mathbf{s}}(x) \cdot \tilde{\mathbf{s}}(x) - c]\nabla_{\mathbf{W}}[\tilde{\mathbf{s}}(x) \cdot \tilde{\mathbf{s}}(x) - c] \\ &= 2[\tilde{\mathbf{s}}^{\mathbf{T}}(x)\tilde{\mathbf{s}}(x) - c]\nabla_{\mathbf{W}}[\tilde{\mathbf{s}}^{\mathbf{T}}(x)\tilde{\mathbf{s}}(x) - c] \\ &= 2[\tilde{\mathbf{s}}^{\mathbf{T}}(x)\tilde{\mathbf{s}}(x) - c]\nabla_{\mathbf{W}}[(\mathbf{W}\bar{\mathbf{s}}(x))^{\mathbf{T}}(\mathbf{W}\bar{\mathbf{s}}(x)) - c] \\ &= 2[\tilde{\mathbf{s}}^{\mathbf{T}}(x)\tilde{\mathbf{s}}(x) - c]\nabla_{\mathbf{W}}[\bar{\mathbf{s}}^{\mathbf{T}}(x)\mathbf{W}^{\mathbf{T}}\mathbf{W}\bar{\mathbf{s}}(x) - c] \\ &= 2[\tilde{\mathbf{s}}^{\mathbf{T}}(x)\tilde{\mathbf{s}}(x) - c][2\mathbf{W}\bar{\mathbf{s}}(x)\bar{\mathbf{s}}^{\mathbf{T}}(x)] \\ &= 4[\tilde{\mathbf{s}}^{\mathbf{T}}(x)\mathbf{W}^{\mathbf{T}}\mathbf{W}\bar{\mathbf{s}}(x) - c][\mathbf{W}\bar{\mathbf{s}}(x)\bar{\mathbf{s}}^{\mathbf{T}}(x)].\end{aligned} \tag{29}$$

Hence, the gradient of the objective function can be expressed as

$$\begin{aligned}\nabla_{\mathbf{W}} J &= \nabla_{\mathbf{W}} J_1 + \nabla_{\mathbf{W}} J_2 \\ &= 2[\mathbf{q}^{\mathbf{T}}\mathbf{W}\bar{\mathbf{s}}(x)][\mathbf{q}\bar{\mathbf{s}}^{\mathbf{T}}(x)] + 4[\tilde{\mathbf{s}}^{\mathbf{T}}(x)\mathbf{W}^{\mathbf{T}}\mathbf{W}\bar{\mathbf{s}}(x) - c] \\ &\quad \times [\mathbf{W}\bar{\mathbf{s}}(x)\bar{\mathbf{s}}^{\mathbf{T}}(x)].\end{aligned} \tag{30}$$

Therefore, the derived BCI algorithm can be expressed as

$$\begin{aligned}\hat{\mathbf{W}}_{\mathbf{p}+1} = \hat{\mathbf{W}}_{\mathbf{p}} - \eta\{&2[\mathbf{q}^{\mathbf{T}}\mathbf{W}_{\mathbf{p}}\bar{\mathbf{s}}(x)][\mathbf{q}\bar{\mathbf{s}}^{\mathbf{T}}(x)] \\ &+ 4[\tilde{\mathbf{s}}^{\mathbf{T}}(x)\mathbf{W}_{\mathbf{p}}^{\mathbf{T}}\mathbf{W}_{\mathbf{p}}\bar{\mathbf{s}}(x) - c][\mathbf{W}_{\mathbf{p}}\bar{\mathbf{s}}(x)\bar{\mathbf{s}}^{\mathbf{T}}(x)]\}.\end{aligned} \tag{31}$$

Because every point of signal $\tilde{\mathbf{s}}(x)$ needs to satisfy Eqs. (21) and (22), we can sequentially and recursively use all the points from 1 to N until the algorithm has converged. That is, for the $\mathbf{p}$th time iteration, we can use the point at $x=(\mathbf{p}-1)\%N+1$, where % is the modulus operator, to calculate the gradient by using Eq. (30).

In addition, for initialization of $\mathbf{W}$, we can simply set $\mathbf{W}_1$ to be an identity matrix, which corresponds to the case where there is no demixing for each channel:

$$\mathbf{W}_1 = \begin{bmatrix} 1 & 0 & 0 \\ 0 & 1 & 0 \\ 0 & 0 & 1 \end{bmatrix}. \tag{32}$$

5. SIMULATIONS AND EXPERIMENTS

A. Simulations

For simulation, we use a paraboloid object surface whose maximum height is 160 mm, which is shown in Fig. 5(d) below. As mentioned in Section 2, the ideal fringe pattern to project onto the reference plane is expressed by Eq. (1). In our simulation, we assume $b_0=128$ and $b_1=100$:

$$s_m(x) = 128 + 100\cos\left(2\pi f_0 x + \frac{2\pi(m-1)}{3}\right) \quad \text{for } m = 1,2,3, \tag{33}$$

where f_0 is the spatial frequency of the fringe pattern, which is assumed to be 10/m in our simulation, and so the spatial period of the fringe pattern is assumed to be 100 mm. Meanwhile, we assume l_0 and d_0 in Fig. 1 equal to 5 m and 2 m, respectively. The spatial resolution of the captured image is assumed to be 1 pixel/mm. Meanwhile, as mentioned in Section 3, we set the expected value of amplitudes of demixed signals at 10, which corresponds to $c=150$.

Additionally, for clarity of comparison, we demonstrate the fringe patterns and the reconstruction results using their cross sections.

1. Color Cross Talk without Nonlinear Distortion

If there is no nonlinear distortion in the system, the reconstruction results will be influenced only by the color cross talk. In this situation, the functions f and g in Fig. 2 are linear functions, and we assume that the cross-talk matrix $\mathbf{A}$ is

$$\mathbf{A} = \begin{bmatrix} 0.5 & 0.1 & 0.2 \\ 0.2 & 0.6 & 0.15 \\ 0.3 & 0.2 & 0.7 \end{bmatrix}. \tag{34}$$

Hence, the captured fringe pattern $\hat{\mathbf{s}} = \mathbf{A} \times \mathbf{s}$. Further, as no higher order harmonic is introduced, low-pass filtering will not be necessary. Thus, the fundamental components of the mixed signals $\bar{\mathbf{s}}$ after the zero-mean operation are shown in Fig. 3(a). We can see that the mixed signals in the color channels have different amplitudes and unbalanced phase shifts. The reconstruction result using this fringe pattern is shown in Fig. 3(b).

In contrast, after estimating the demixing matrix $\mathbf{W}$ by Eq. (31), the demixed signal $\tilde{\mathbf{s}} = \mathbf{W} \times \bar{\mathbf{s}}$ is shown in Fig. 4(a): It can be seen that after the demixing, the output signal $\tilde{\mathbf{s}}$ has been completely balanced. The corresponding reconstruction results are plotted in Fig. 4(b) by the solid curve, and the dashed curve is the true value of the height

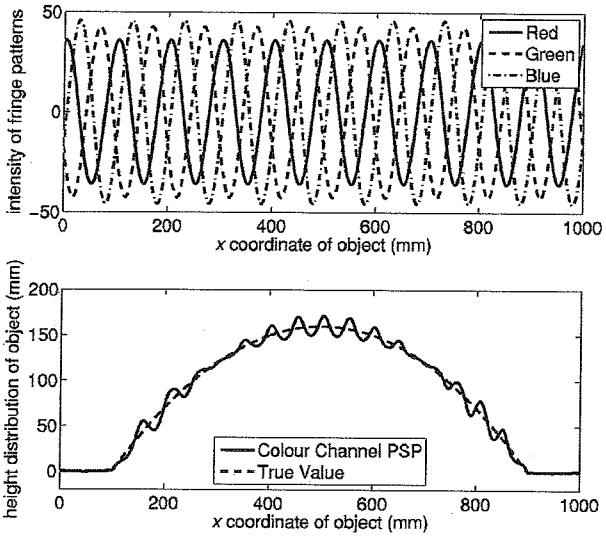

Fig. 3. Linearly mixed fringe patterns and reconstruction result.

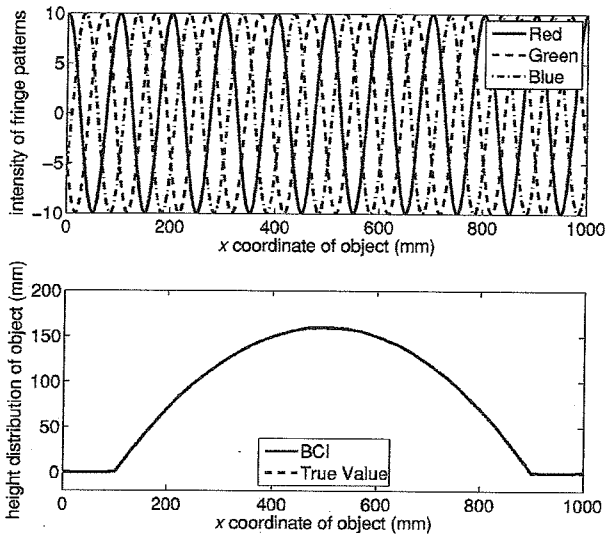

Fig. 4. Demixed fringe pattern and reconstruction result in the linear cross-talk situation.

distribution. We can see that the result is almost identical to the true value and that the reconstruction error has been significantly reduced.

2. Color Cross Talk with Nonlinear Distortions

In the nonlinear color cross-talk situation, we assume the nonlinear function f in Fig. 2 to be

$$f(s) = 128\frac{\tanh(3s/128 - 3)}{\tanh(3)} + 128, \tag{35}$$

which is mapping the values from range [0,256] to range [0,256] and is plotted in Fig. 5(a). The mixing matrix is the same with the linear mixing situation, which is given by Eq. (34). Further, we assume that the nonlinear function g is a quadratic function:

$$g(s) = s^2/256, \tag{36}$$

which is a nonlinear function mapping the values from range [0,256] to range [0,256] as well.

Based on the assumed nonlinear functions f, g and the mixing matrix $\mathbf{A}$, the captured fringe pattern on the reference plane and the surface of the object can be calculated accordingly. The simulated fringe patterns $\hat{\mathbf{s}}$ and $\hat{\mathbf{d}}$ are shown in Figs. 5(b) and 5(c), respectively.

For clarity, a cross section of the fringe pattern $\hat{\mathbf{s}}$ is shown in Fig. 6(a). We can see that the captured fringe pattern $\hat{\mathbf{s}}$ is highly distorted by nonlinear functions and the color cross talk. By using these fringe patterns, the reconstruction result is shown in Fig. 6(b) by the solid

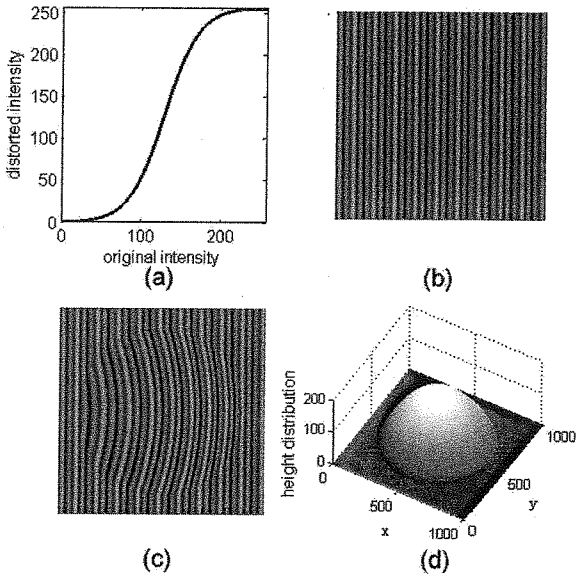

Fig. 5. (Color online) Simulated fringe patterns and object.

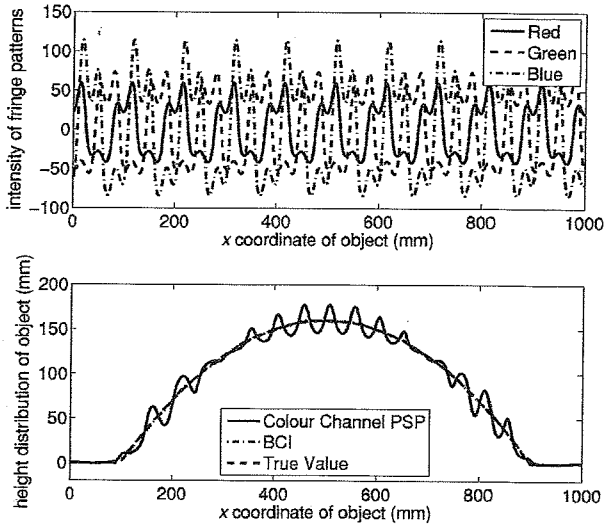

Fig. 6. Cross section of captured fringe patterns with nonlinear color cross talk and reconstruction result.

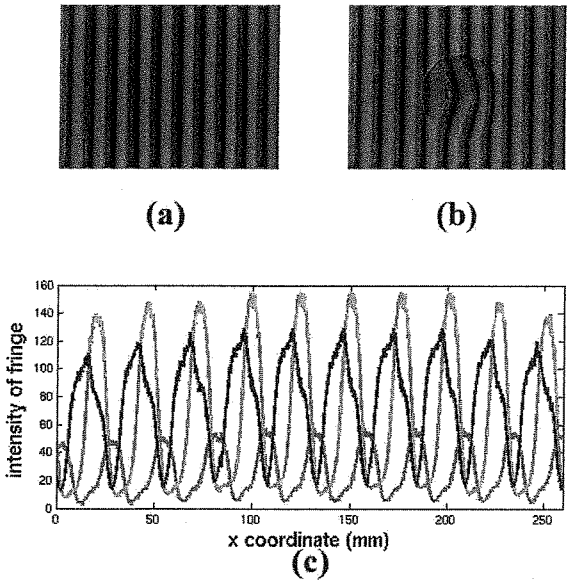

Fig. 7. (Color online) Object and fringe patterns in the experiment.

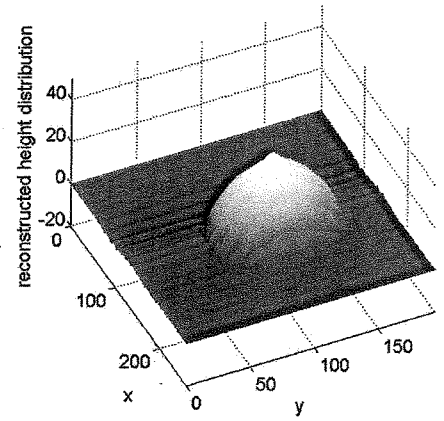

Fig. 8. Surface reconstructed by color channel PSP.

curve. The true value is plotted by the dashed curve. In contrast, after low-pass filtering and demixing by using the BCI algorithm, a very accurate reconstruction result can be achieved as shown by dashed curve in Fig. 6(b), which is almost identical to the true value of the profile.

B. Experiment

In our experiments, the fringes were projected using an InFocus LP530 DLP projector at a distance of 2 m from the reference plane. The images were captured by a DuncanTech MS3100-RGB3 CCD located 81 cm from the projector and connected to a computer, which is used to try to generate sinusoidal fringes. The object to be measured was a cone on the reference plane as shown in Fig. 7(b). The height of the cone is 38 mm, and the diameter of the bottom surface of the cone is 94 mm. Figures 7(a) and 7(b) are the captured fringes on the reference plane and on the object surface, respectively. As mentioned above, because of the nonlinear distortion and the color cross talk, the captured fringe pattern on the reference plane becomes nonsinusoidal and unbalanced, as shown in Fig. 7(c), where the plotted signal is a cross section of Fig. 7(a). It can be seen that the amplitudes of the fringe pattern in each channel are different and that the fringe patterns are nonlinearly distorted and color cross talked. In our experiment, the resolution of the CCD camera is 1392 $\times$1039 pixels. The field of vision for CCD camera is 260 mm$\times$194 mm. Hence, the equivalent spatial resolution is 0.1868 mm/pixel. The equivalent spatial period of the projected fringe was 25.7 mm, i.e., f_0=38.9/m.

The reconstruction result achieved without color demixing is shown in Fig. 8. We can see that the reconstructed profile without color demixing has the shape of a spherical cap with a jagged and rough surface. In contrast, by using the BCI algorithm, an accurately reconstructed cone with a very straight edge profile and smooth surface is obtained, as shown in Fig. 9.

More clearly, a comparison of the reconstructed surfaces in cross-section view is shown in Fig. 10, where solid and dashed curves represent the measurement results by using color-channel-based PSP without and with the BCI algorithm, respectively. As normally the cross sections of a cone are parabolas, and the only exception is its central cross section, which is a triangle, in Fig. 10 we select two cross sections of the cone, the central cross section and a cross section with half height of the cone, to demonstrate the measurement results.

Further, in order to quantitatively compare the measurement accuracy with and without BCI in the experi-

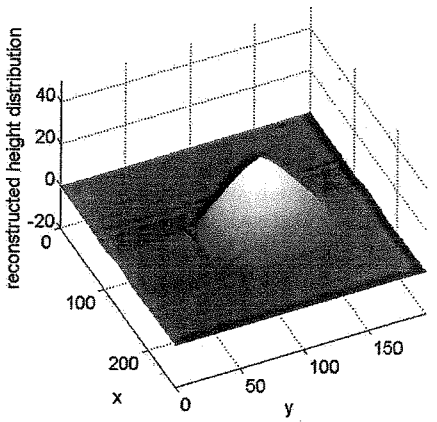

Fig. 9. Surface reconstructed by BCI.

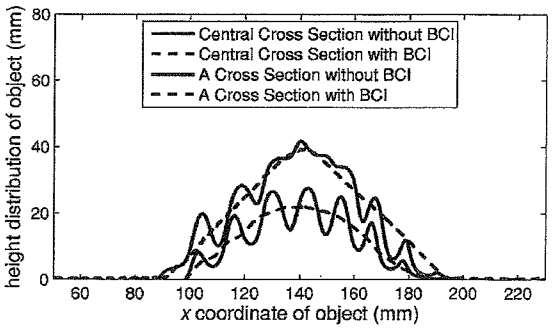

Fig. 10. Comparison of the reconstructed surfaces in the experiment in cross-section view.

Table 1. Absolute Error and Standard Deviation

Color Channel PSP	ε_a (mm)	ε_s (mm)
With BCI	0.7976	0.6303
Without BCI	3.1418	3.8874

ment, the average absolute error ε_a and the standard deviation ε_s of the two different cases are listed in Table 1. Both visual and quantitative comparison confirm that reconstruction errors can be significantly reduced by using our proposed BCI algorithm.

6. CONCLUSION

In this paper, we first proposed a general color mixing model to describe the color cross-talk phenomenon and theoretically analyzed the errors introduced by the color leakage when the color-channel-based PSP technique is utilized. Then, based on the proposed model and analysis, we presented a method, called blind color isolation (BCI), to reduce the influence of color cross talk for color-channel-based PSP. BCI is a pure "blind" and adaptive approach to effectively decoupling the cross talk among color channels without knowing the characteristics of the digital projector and the CCD camera. Moreover, no extra calibration process is required to determine the demixing matrix. Simulation and experimental results have confirmed that the proposed general model works for practical situations. Meanwhile, the presented BCI can effectively eliminate color cross talk and, further, significantly improve the measurement accuracy for color-channel-based PSP.

APPENDIX A: INFLUENCE OF NONLINEAR DISTORTION

Theorem 1. If a signal $s(x)$ can be expressed in the form of a linear combination of a fundamental component $\cos\theta(x)$ and its integral-order harmonics, i.e.,

$$s(x)=\sum_{k=0}^{P}[p_k\cdot\cos(k\cdot\theta(x))], \tag{A1}$$

then the nonlinear distortion of $s(x)$ can be also approximated by

$$g(s(x))=\sum_{k=0}^{R}[r_k\cdot\cos(k\cdot\theta(x))]. \tag{A2}$$

Proof: A nonlinear function $g(s)$ can always be sufficiently approximated by a polynomial whose order N is sufficiently large:

$$g(s)=\sum_{n=0}^{N}g_n s^n=g_0+g_1 s+g_2 s^2+\cdots+g_n s^n+\cdots+g_N s^N, \tag{A3}$$

where g_n is the coefficient of the term of s^n. Hence, we need only to prove that every term s^n can be expressed as a linear combination of a fundamental component $\cos\theta(x)$ and its integral-order harmonics. It can be proved by using mathematical induction:

1. It is obvious that when $n=1$ the proposition is true.
2. Assume that when $n=m$, the proposition is true, i.e.,

$$s^m(x)=\sum_{j=0}^{Q}[q_j\cdot\cos(j\cdot\theta(x))]. \tag{A4}$$

3. For the term $s^{m+1}(x)$, we can have

$$\begin{aligned}s^{m+1}(x)&=s^m(x)\cdot s(x)\\&=\sum_{j=0}^{Q}[q_j\cdot\cos(j\cdot\theta(x))]\cdot\sum_{k=0}^{K}[p_k\cdot\cos(k\cdot\theta(x))]\\&=\sum_{j=0}^{Q}\sum_{k=0}^{K}q_j p_k\cos(j\cdot\theta(x))\cos(k\cdot\theta(x))\\&=\frac{1}{2}\sum_{j=0}^{Q}\sum_{k=0}^{K}q_j p_k\{\cos[(j+k)\cdot\theta(x)]+\cos[(j-k)\cdot\theta(x)]\}\\&=\frac{1}{2}\sum_{j=1}^{Q}\sum_{k=0}^{K}q_j p_k\cos[(j+k)\cdot\theta(x)]\\&\quad+\frac{1}{2}\sum_{j=0}^{Q}\sum_{k=0}^{K}q_j p_k\cos[(j-k)\cdot\theta(x)].\end{aligned} \tag{A5}$$

Obviously, every term $s^{m+1}(x)$ contains only the integral-order harmonics of $\cos\theta(x)$. Hence, $s^{m+1}(x)$ can be also expressed as

$$s^{m+1}(x)=\sum_{k=0}^{R}[i_k\cdot\cos(k\cdot\theta(x))]. \tag{A6}$$

Therefore, Theorem 1 is proved.

Corollary 1. Nested nonlinear distortion of $s(x)$ can be also approximated in the same form, i.e.,

$$g_n(\ldots g_2[g_1(s)])=\sum_{k=0}^{L}[l_k\cdot\cos(k\cdot\theta(x))]. \tag{A7}$$

APPENDIX B: PROOF OF NECESSARY AND SUFFICIENT CONDITION FOR BALANCED SIGNALS

Theorem 2. Equations (21) and (22) are the necessary and sufficient conditions for $\tilde{\mathbf{s}}$ to be a set of three balanced signals, where $\tilde{\mathbf{s}}$ is given by

$$\tilde{\mathbf{s}}_m=\tilde{b}_{m,1}\cos(\theta(x)+\tilde{\alpha}_m),\quad \text{for } m=1,2,3, \tag{B1}$$

where $\tilde{b}_{m,1}>0$ denotes the amplitude of the signal and

$$0\le\tilde{\alpha}_1<\tilde{\alpha}_2<\tilde{\alpha}_3<2\pi. \tag{B2}$$

Proof: It can be easily verified that if $\tilde{\mathbf{s}}$ is a set of three balance signals, i.e., if we have

$$\tilde{b}_{m,1} = \tilde{b}, \tag{B3}$$

$$\tilde{\alpha}_3 - \tilde{\alpha}_2 = \tilde{\alpha}_2 - \tilde{\alpha}_1 = 2\pi/3, \tag{B4}$$

$\tilde{\mathbf{s}}$ satisfies Eqs. (21) and (22):

$$\mathbf{q} \cdot \tilde{\mathbf{s}}(x) = 0 \text{ for any given } x, \tag{B5}$$

$$\tilde{\mathbf{s}}(x) \cdot \tilde{\mathbf{s}}(x) = \frac{3}{2}\tilde{b}^2 = c \text{ for any given } x. \tag{B6}$$

Therefore, the necessity of Eqs. (21) and (22) has been proved. Thus, we need only to prove the sufficiency of Eqs. (21) and (22).

From Eqs. (21) and (22), we can have

$$\frac{\mathbf{d}[\mathbf{q} \cdot \tilde{\mathbf{s}}(x)]}{\mathbf{d}x} = 0 \text{ for any given } x, \tag{B7}$$

$$\frac{\mathbf{d}[\tilde{\mathbf{s}}(x) \cdot \tilde{\mathbf{s}}(x)]}{\mathbf{d}x} = 0 \text{ for any given } x; \tag{B8}$$

i.e.,

$$\frac{\mathbf{d}\theta(x)}{\mathbf{d}x} \sum_{m=1}^{3} \tilde{b}_{m,1} \sin[\theta(x) + \tilde{\alpha}_m] = 0, \tag{B9}$$

and

$$\begin{aligned}
&\sum_{m=1}^{3} \frac{\mathbf{d}(\tilde{b}_{m,1}^2 \sin^2[\theta(x) + \tilde{\alpha}_m])}{\mathbf{d}x} \\
&= \sum_{m=1}^{3} \frac{\mathbf{d}(\tilde{b}_{m,1}^2 \sin^2[\theta(x) + \tilde{\alpha}_m])}{\mathbf{d}\theta} \cdot \frac{\mathbf{d}\theta(x)}{\mathbf{d}x} \\
&= \frac{\mathbf{d}\theta(x)}{\mathbf{d}x} \sum_{m=1}^{3} \frac{\mathbf{d}(\tilde{b}_{m,1}^2 \sin^2[\theta(x) + \tilde{\alpha}_m])}{\mathbf{d}\theta} \\
&= \frac{\mathbf{d}\theta(x)}{\mathbf{d}x} \sum_{m=1}^{3} 2\tilde{b}_{m,1}^2 \cos[\theta(x) + \tilde{\alpha}_m] \sin[\theta(x) + \tilde{\alpha}_m] \\
&= \frac{\mathbf{d}\theta(x)}{\mathbf{d}x} \sum_{m=1}^{3} \tilde{b}_{m,1}^2 \sin[2\theta(x) + 2\tilde{\alpha}_m] = 0.
\end{aligned} \tag{B10}$$

As $\theta(x)$ denotes $2\pi f_0 x$, $\mathbf{d}\theta(x)/\mathbf{d}x = 2\pi f_0 \neq 0$, we have

$$\sum_{m=1}^{3} \tilde{b}_{m,1} \sin[\theta(x) + \tilde{\alpha}_m] = 0, \tag{B11}$$

$$\sum_{m=1}^{3} \tilde{b}_{m,1}^2 \sin[2\theta(x) + 2\tilde{\alpha}_m] = 0. \tag{B12}$$

For simplicity of the expression, let $\tilde{b}_m = \tilde{b}_{m,1} > 0$ and $\beta_m = \tilde{\alpha}_m - \tilde{\alpha}_1$. Obviously $\beta_1 = 0$, and accordingly Eqs. (B11) and (B12) can be simplified:

$$\sum_{m=1}^{3} \tilde{b}_m \sin(\theta + \beta_m) = 0, \tag{B13}$$

$$\sum_{m=1}^{3} \tilde{b}_m^2 \sin(2\theta + 2\beta_m) = 0. \tag{B14}$$

In addition, according to Eq. (B2), we have

$$\tilde{\alpha}_1 - \tilde{\alpha}_1 < \tilde{\alpha}_2 - \tilde{\alpha}_1 < \tilde{\alpha}_3 - \tilde{\alpha}_1 < 2\pi, \tag{B15}$$

i.e.,

$$0 < \beta_2 < \beta_3 < 2\pi. \tag{B16}$$

Because Eqs. (B13) and (B14) always hold for any given x, when $x=0$, $\theta = 2\pi f_0 x = 0$, we can have

$$\tilde{b}_2 \sin(\beta_2) + \tilde{b}_3 \sin(\beta_3) = 0, \tag{B17}$$

$$\tilde{b}_2^2 \sin(2\beta_2) + \tilde{b}_3^2 \sin(2\beta_3) = 0, \tag{B18}$$

i.e.,

$$\tilde{b}_2 \sin(\beta_2) = -\tilde{b}_3 \sin(\beta_3), \tag{B19}$$

$$\tilde{b}_2^2 \sin(2\beta_2) = -\tilde{b}_3^2 \sin(2\beta_3). \tag{B20}$$

Meanwhile, as $\tilde{b}_m > 0$, it is not difficult to verify that $\sin(\beta_2) \neq 0$ and $\sin(\beta_3) \neq 0$, because if $\sin(\beta_2) = 0$, we will have $\sin(\beta_3) = 0$ by Eq. (B19). Thus, we have $\beta_2 = k\pi$ and $\beta_3 = n\pi$, where k and n are integers. Hence, from Eq. (B14), we can have

$$\tilde{b}_1^2 \sin(2\theta) + \tilde{b}_2^2 \sin(2\theta + 2k\pi) + \tilde{b}_3^2 \sin(2\theta + 2n\pi) = 0, \tag{B21}$$

i.e.,

$$(\tilde{b}_1^2 + \tilde{b}_2^2 + \tilde{b}_3^2)\sin(2\theta) = 0. \tag{B22}$$

As $\sin(2\theta)$ can be arbitrary values, we have to require $(\tilde{b}_1^2 + \tilde{b}_2^2 + \tilde{b}_3^2) = 0$, which contradict $\tilde{b}_m > 0$.

Therefore, as both sides of Eq. (B19) are not zeros, dividing Eq. (B20) by Eq. (B19), we obtain

$$\frac{\tilde{b}_2^2 \sin(2\beta_2)}{\tilde{b}_2 \sin(\beta_2)} = \frac{\tilde{b}_3^2 \sin(2\beta_3)}{\tilde{b}_3 \sin(\beta_3)}, \tag{B23}$$

i.e.,

$$\tilde{b}_2 \cos(\beta_2) = \tilde{b}_3 \cos(\beta_3). \tag{B24}$$

Further, from Eqs. (B24) and (B19), we have

$$[\tilde{b}_2 \sin(\beta_2)]^2 + [\tilde{b}_2 \cos(\beta_2)]^2 = [-\tilde{b}_3 \sin(\beta_3)]^2 + [\tilde{b}_3 \cos(\beta_3)]^2 \tag{B25}$$

i.e.,

$$\tilde{b}_2^2 = \tilde{b}_3^2. \tag{B26}$$

As $b_m > 0$, we have

$$\tilde{b}_2 = \tilde{b}_3. \tag{B27}$$

Similarly, considering the cases when $x=-\beta_2/(2\pi f_0)$ and $x=-\beta_3/(2\pi f_0)$, i.e., when $\theta=-\beta_2$ and $\theta=-\beta_3$, we can have $\tilde{b}_1=\tilde{b}_3$ and $\tilde{b}_1=\tilde{b}_2$, respectively. Therefore, $\tilde{b}_1=\tilde{b}_2=\tilde{b}_3=\tilde{b}>0$, where $\tilde{b}$ is a positive constant. Thus, Eqs. (B13) and (B14) can be further simplified as

$$\tilde{b}\sum_{m=1}^{3}\sin(\theta+\beta_m)=0, \tag{B28}$$

$$\tilde{b}^2\sum_{m=1}^{3}\sin(2\theta+2\beta_m)=0, \tag{B29}$$

i.e.,

$$\sum_{m=1}^{3}\sin(\theta+\beta_m)=0, \tag{B30}$$

$$\sum_{m=1}^{3}\sin(2\theta+2\beta_m)=0. \tag{B31}$$

When $\theta=\pi/2$, Eq. (B30) becomes

$$\sin(\pi/2)+\sin(\pi/2+\beta_2)+\sin(\pi/2+\beta_3)=0, \tag{B32}$$

i.e.,

$$1+\cos(\beta_2)+\cos(\beta_3)=0. \tag{B33}$$

Since $\tilde{b}_2=\tilde{b}_3=\tilde{b}>0$, by Eq. (B24) we have

$$\cos(\beta_2)=\cos(\beta_3). \tag{B34}$$

Hence, substituting this equation into Eq. (B33), we can have

$$1+2\cos(\beta_2)=0 \quad \text{and} \quad 1+2\cos(\beta_3)=0, \tag{B35}$$

i.e.,

$$\cos(\beta_2)=-1/2 \quad \text{and} \quad \cos(\beta_3)=-1/2. \tag{B36}$$

Therefore,

$$\beta_2=2\pi/3 \quad \text{or} \quad \frac{4\pi}{3} \quad \text{and} \quad \beta_3=2\pi/3 \quad \text{or} \quad 4\pi/3. \tag{B37}$$

Meanwhile, according to Eq. (B16), $\beta_2<\beta_3$, the final solution is $\beta_2=2\pi/3$, $\beta_3=4\pi/3$. Therefore,

$$\alpha_2-\alpha_1=\beta_2=2\pi/3, \tag{B38}$$

$$\alpha_3-\alpha_2=(\alpha_3-\alpha_1)-(\alpha_2-\alpha_1)=\beta_3-\beta_2=2\pi/3. \tag{B39}$$

Now we have proved that

$$\tilde{b}_1=\tilde{b}_2=\tilde{b}_3=\tilde{b},$$

$$\alpha_3-\alpha_2=\alpha_2-\alpha_1=2\pi/3,$$

which implies that $\tilde{s}_m$ $(m=1,2,3)$ is a set of balanced signals. Therefore, the sufficiency has been proved.

REFERENCES

1. M. Takeda and K. Mutoh, "Fourier transform profilometry for the automatic measurement of 3-D object shapes," Appl. Opt. **22**, 3977–3982 (1983).
2. M. Takeda, H. Ina, and S. Kobayashi, "Fourier-transform method of fringe-pattern analysis for computer-based topography and interferometry," J. Opt. Soc. Am. **72**, 156–160 (1982).
3. R. J. Green, J. G. Walker, and D. W. Robinson, "Investigation of the Fourier-transform method of fringe pattern analysis," Opt. Lasers Eng. **8**, 29–44 (1988).
4. X. Su and W. Chen, "Fourier transform profilometry: a review," Opt. Lasers Eng. **35**, 263–284 (2001).
5. J. Yi and S. Huang, "Modified Fourier transform profilometry for the measurement of 3-D steep shapes," Opt. Lasers Eng. **27**, 493–505 (1997).
6. X. Su, W. Chen, Q. Zhang, and Y. Chao, "Dynamic 3-D shape measurement method based on ftp," Opt. Lasers Eng. **36**, 49–64 (2001).
7. V. Srinivasan, H. Liu, and M. Halioua, "Automated phase-measuring profilometry of 3-D diffuse objects," Appl. Opt. **23**, 3105–3108 (1984).
8. X. Su, W. Zhou, G. von Bally, and D. Vukicevic, "Automated phase-measuring profilometry using defocused projection of ronchi grating," Opt. Commun. **94**, 561–573 (1992).
9. H. Su, J. Li, and X. Su, "Phase algorithm without the influence of carrier frequency," Opt. Eng. (Bellingham) **36**, 1799–1805 (1997).
10. S. Toyooka and Y. Iwaasa, "Automatic profilometry of 3-D diffuse objects by spatial phase detection," Appl. Opt. **25**, 1630–1633 (1986).
11. R. Rodriguez-Vera and M. Servin, "Phase locked loop profilometry," Opt. Laser Technol. **26**, 393–398 (1994).
12. A. J. Moore and F. Mendoza-Santoyo, "Phase demodulation in the space domain without a fringe carrier," Opt. Lasers Eng. **23**, 319–330 (1995).
13. J. Villa, M. Servin, and L. Castillo, "Profilometry for the measurement of 3-D object shapes based on regularized filters," Opt. Commun. **161**, 13–18 (1999).
14. P. Huang, Q. Ho, F. Jin, and F. Chiang, "Colour-enhanced digitial fringe projection technique for high-speed 3-D surface contouring," Opt. Eng. (Bellingham) **38**, 1065–1071 (1999).
15. L. Kinell, "Multichannel method for absolute shape measurement using projected fringes," Opt. Lasers Eng. **41**, 57–71 (2004).
16. Y. Hu, J. Xi, E. Li, J. Chicharo, and Z. Yang, "A calibration approach for decoupling colour cross-talk using nonlinear blind signal separation network," in *Proceedings of IEEE Conference on Optoelectronic and Microelectronic Materials and Devices (COMMAD)* (IEEE, 2004), pp. 265–268.
17. F. Berryman, P. Pynsent, and J. Cubillo, "A theoretical comparison of three fringe analysis method for determining the three dimensional shape of an object in the presence of noise," Opt. Lasers Eng. **39**, 35–50 (2003).
18. K. Hibino, B. F. Oreb, and D. I. Farrant, "Phase shifting for nonsinusoidal waveforms with phase-shift errors," J. Opt. Soc. Am. A **12**, 761–768 (1995).
19. J. E. Greivenkamp, "Generalized data reduction for heterodyne interferometry," Opt. Eng. (Bellingham) **23**, 350–352 (1984).
20. G. Stoilov and T. Dragostinov, "Phase-stepping interferometry: five-frame algorithm with an aribitrary step," Opt. Lasers Eng. **28**, 61–69 (1997).
21. G.-S. Han and S.-W. Kim, "Numerical correction of reference phases in phase-shifting interferometry by iterative least-squares fitting," Appl. Opt. **33**, 7321–7325 (1994).
22. G. Lai and T. Yatagai, "Generalized phase-shifting interferometry," J. Opt. Soc. Am. A **8**, 822–827 (1991).
23. X. Chen, M. Gramaglia, and J. A. Yeazell, "Phase-shifting interferometry with uncalibrated phase shifts," Appl. Opt. **39**, 585–591 (2000).
24. H. Kadono, Y. Bitoh, and S. Toyooka, "Statistical

interferometry based on a fully developed speckle field: an experimental demonstration with noise analysis," J. Opt. Soc. Am. A **18**, 1267–1274 (2001).
25. C. S. Guo and L. Zhang, "Phase-shifting error and its elimination in phase-shifting digital holography," Opt. Lett. **27**, 1687–1689 (2002).
26. L. Z. Cai, Q. Liu, and X. L. Yang, "Phase-shift extraction and wave-front reconstruction in phase-shifting interferometry with arbitrary phase steps," Opt. Lett. **28**, 1808–1810 (2003).
27. L. Z. Cai, Q. Liu, and X. L. Yang, "Generalized phase-shifting interferometry with arbitrary unknown phase steps for diffraction objects," Opt. Lett. **29**, 183–185 (2004).
28. Y. Hu, J. Xi, E. Li, J. Chicharo, and Z. Yang, "Three-dimensional profilometry based on shift estimation of projected fringe patterns," Appl. Opt. **45**, 678–687 (2006).